Why pens have rubbery grips

Brygida Dzidek[a], Séréna Bochereau[b], Simon A. Johnson[c], Vincent Hayward[b], and Michael J. Adams[a,1]

[a]School of Engineering, University of Birmingham, Birmingham B15 2TT, United Kingdom; [b]Sorbonne Universités, Université Pierre et Marie Curie Univ Paris 06, Institut des Systèmes Intelligents et de Robotique, F-75005 Paris, France; and [c]Unilever Research & Development Port Sunlight, Bebington, Wirral CH63 3JW, United Kingdom

Edited by David A. Weitz, Harvard University, Cambridge, MA, and approved August 22, 2017 (received for review April 14, 2017)

The process by which human fingers gives rise to stable contacts with smooth, hard objects is surprisingly slow. Using high-resolution imaging, we found that, when pressed against glass, the actual contact made by finger pad ridges evolved over time following a first-order kinetics relationship. This evolution was the result of a two-stage coalescence process of microscopic junctions made between the keratin of the stratum corneum of the skin and the glass surface. This process was driven by the secretion of moisture from the sweat glands, since increased hydration in stratum corneum causes it to become softer. Saturation was typically reached within 20 s of loading the contact, regardless of the initial moisture state of the finger and of the normal force applied. Hence, the gross contact area, frequently used as a benchmark quantity in grip and perceptual studies, is a poor reflection of the actual contact mechanics that take place between human fingers and smooth, impermeable surfaces. In contrast, the formation of a steady-state contact area is almost instantaneous if the counter surface is soft relative to keratin in a dry state. It is for this reason that elastomers are commonly used to coat grip surfaces.

finger friction | true contact area kinetics | biotribology | fingerprints

We often take it for granted that our fingers instantly bring about continuous contact when they touch smooth objects. The fingerprint marks remaining on these objects after detachment, however, are the record of a surprisingly slow process. During a period of many seconds, several phenomena take place at different length scales and timescales that eventually lead to a stable contact state, where the flattened apices of the ridges establish a uniform contact with the counter surface. Here, we observed that the so-called "true contact area," which quantifies the amount of material in intimate contact (i.e., in atomic proximity) (1, 2), varies dynamically over a period of many seconds, while the apparent, or gross, contact area, by and large, remains unchanged through time.

A knowledge of the evolution of a contact is informative, because a true contact area determines the creation of friction, which is so essential to everyday life. Without a large true contact area made by our hands, it would be nearly impossible to lift a glass or to hold onto a handrail in a transport vehicle. Recent tactile display technologies depend crucially on the development of friction between a finger and a glass surface (3, 4). Some powerful tactile illusions are the direct consequence of the differential frictional properties of surfaces across space (5), and astonishing human perceptual performance in the discrimination of materials can be explained by subtle variations in frictional properties (6). Thus, there is ample motivation for investigating the details of the formation of the true contact area by fingertips in contact with smooth surfaces.

The superficial layer of human finger pads that is in direct contact with objects, termed the stratum corneum, is made in a large proportion of keratin (keratinized cells), one of the most abundant structural materials in animals. The keratin of the stratum corneum is a composite material that comprises a mix of molecules in a crystalline state and those in an amorphous state. The crystalline component is impervious to the effect of water, and therefore, it can preserve its gross shape. The amorphous component, however, is avid of water, and the presence or absence of water profoundly modifies its mechanical properties (7). Dry stratum corneum has an elastic modulus of about 1 GPa, but this value can be reduced by approximatively four orders of magnitude when it is saturated with water (8). In the wet state, stratum corneum can yield 150% of its original length at almost constant stress, giving it plasticity (9).

The macroscopic geometry of the finger pad, which is characterized by ridges and valleys that compress, decompress, and stretch during interactions with surfaces, undergoes considerable gross deformation even for moderate contact loads (10). The surfaces of the ridges exhibit roughly cylindrical cross-sections and are separated by valleys (8). They form loops, whorls, or arch patterns that are unique to each individual.

The evolution of the apparent area of contact arising from the deformation of a finger pad has been examined using optical imaging during incipient slip (11); at different force levels (12, 13); at different moisture contents (14) and tangential loads leading to slip (15); under rotation and lateral sliding movements over flat, raised, or indented glass surfaces (10); during stick-to-slip transitions in distal, proximal, radial, and ulnar directions (16); over complete stick-to-slip epochs (17); and under the effects of oscillating loads (18, 19).

Previous studies considered the area of a finger pad contact macroscopically. A contact was typically described by an apparent, or gross, area and then, by excluding the interstitial spaces between the ridges in an effort to better approximate the true contact area. Thus, the total contact area made by the ridges compared with the gross area would quantify their overall deformation, since these two values would coincide if the ridges were completely deformed.

The ridges themselves are far from being smooth and exhibit small-scale topographical features. In a recent study (20), the

ENGINEERING

Significance

Why does gripping a pen, tool, or handle feel more secure when it is coated with a rubbery material? The keratin of the skin outer layer is stiff and rough at a small scale. When encountering a smooth, stiff, and impermeable surface, such as polished metal or glass, the actual contact area is initially small as is the friction. Because the keratin softens when it is hydrated by the moisture secreted from the sweat pores, it requires many seconds for the contact area to increase to the value reached almost instantaneously with a soft material, such as a rubber. This mechanism might be used by our tactile sense to identify materials and has implications for the design of tactile displays.

Author contributions: B.D., S.B., S.A.J., V.H., and M.J.A. designed research; B.D., S.B., S.A.J., V.H., and M.J.A. performed research; B.D., S.B., S.A.J., and M.J.A. analyzed data; B.D. and S.B. conducted the experiments and analyzed the results; B.D., S.B., S.A.J., V.H., and M.J.A. discussed the results; and B.D., S.B., S.A.J., V.H., and M.J.A. wrote the paper.

The authors declare no conflict of interest.

This article is a PNAS Direct Submission.

Freely available online through the PNAS open access option.

[1]To whom correspondence should be addressed. Email: m.j.adams@bham.ac.uk.

This article contains supporting information online at www.pnas.org/lookup/suppl/doi:10.1073/pnas.1706233114/-/DCSupplemental.

effect of these features could be, for the first time, observed directly. They initially yielded few unconnected regions within the ridge contacts. The summed areas of these regions, which were described as junctions, corresponded to a total area denoted A_{junct}. The total junction contact area was observed to grow for many seconds during the holding period after a loading event, while the gross and ridge areas, A_{gross} and A_{ridge}, respectively, remained unchanged (20). This growth was the result of a two-step coalescence process, such that the number of junctions, N, first increased followed by their expansion that led to a rise in connectivity. It was surmised that this process was the result of an occlusion mechanism, such that the stratum corneum became gradually plasticized under the action of moisture secreted from the many sweat pores located in the ridges (21). This phenomenon could explain the first-order growth kinetics exhibited by the coefficient of friction (2).

We investigated this newly discovered phenomenon in greater detail by characterizing the influence of the loading forces and the loading rate on its time course. This study provides a basis for establishing a robust description of the evolution of the contact area for steady pressing conditions associated with everyday interactions involving smooth surfaces. The results are contrasted with the case of the contact of a finger pad with an elastomer. With such a counter surface, the kinetics of contact formation exhibit a drastically different behavior, since its relative softness allows a steady-state contact to be reached almost instantaneously.

The observed contact evolutions during interactions with solid surfaces are a tribute to the ability of the human nervous system to secure stable grips and to achieve tactile perceptual constancy, despite the extensive variations in detailed contact mechanics through time during finger contact with objects. They also have important implications for the design of touch screens with haptic feedback that rely on the modulation of friction to provide computer-controlled tactile sensations.

Results

Fingerprint images for two participants were obtained using the technique of frustrated total internal reflection (*Materials and Methods*). The washed and dried pads of their index fingers were slowly pressed against the face of a prism until reaching a maximum normal loading force. The fingers were then held in a fixed isometric condition for 60 s after the maximum normal load was reached. Testing conditions differed by rate of compression, maximum normal load, counter surface material, and participant. Binary images obtained after enhancement and thresholding (*Materials and Methods*) are exemplified in Fig. 1 for different instances after the initial contact. Enlarged image portions more clearly show how the junctions evolved with time. Figs. 2 and 3 show the results of an automated image analysis procedure performed at high resolution (*Materials and Methods*).

Conditions. There were eight testing conditions, labeled from a to h, listed in Table 1. Condition h corresponded to the finger of participant B pressing against a sheet of polydimethylsiloxane (PDMS), a silicone-based transparent elastomer (*Materials and Methods*). Trials carried out with the same finger tested twice under the same conditions have subscripts 1 and 2. Compression rates were 0.5, 1.0, or 2.0 mm s^{-1}, and the maximum normal forces were 2.0 or 3.0 N. The time $t_{\max}$ was the time at which the maximum normal force was reached, and A_{E} represented the relative contact area at the end of the hold period computed as A_{junct} normalized by A_{gross}. The datasets (Table 1) were acquired with very low likelihood that accidental lateral slips of the finger took place during imaging (*Materials and Methods*).

Junction Area Kinetics. Fig. 2 shows the typical evolution of A_{junct} as a function of contact time with glass. During the loading period, the value of A_{gross} increased to a maximum, while the value of A_{junct} increased during the loading and the hold periods. During the hold period at constant compression, the normal force relaxed to less than one-half of its initial value because of the viscoelastic properties of finger tissues (22).

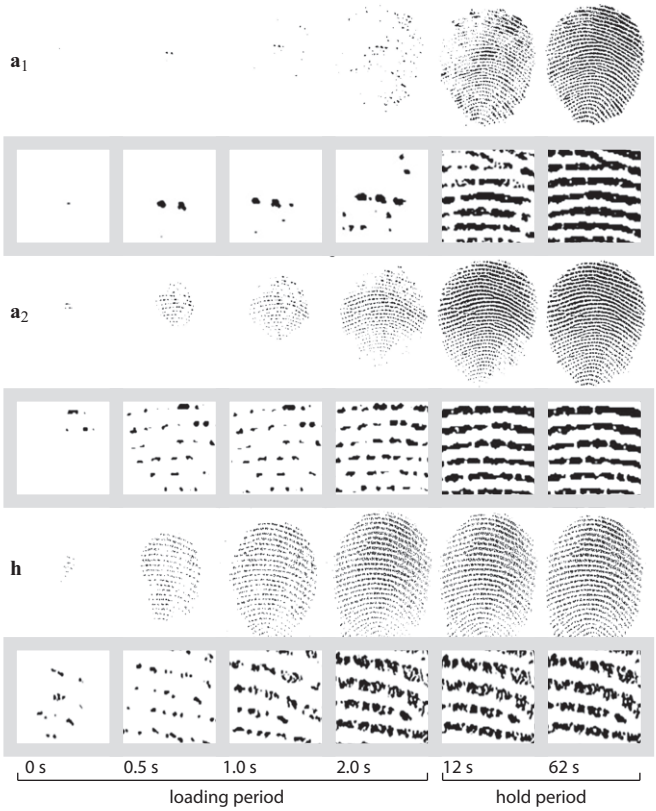

Fig. 1. Temporal evolution of the contact area on a glass surface for participant A corresponding to trials a_1 and a_2 (Table 1). Each row is associated with framed enlarged image portions depicting the creation, growth, and coalescence of regions of the junction area. The last two rows show the contact evolution on a PDMS surface (*Materials and Methods*) under similar conditions for participant B, dataset h.

Fig. 3 shows the temporal evolution of A_{E} and of the junction density, N/A_{gross}, as a function of the hold time, t, for 14 trials. With the exception of trials d_1, d_2, f_1, and b_2, A_{junct} increased relative to A_{gross} at a decreasing rate, such that the data could be adequately described by a first-order kinetics equation:

$$A_{\text{junct}}(t) = A_\infty + (A_0 - A_\infty)\exp\left(-\frac{t}{\lambda}\right), \qquad [1]$$

where λ is the characteristic time and where the subscripts 0 and ∞ refer to the values of A_{junct} at times $t = 0$ and $t \to \infty$.

Junction Area and Junction Density Kinetics. Fitting the parameters A_∞, A_0, and λ of Eq. **1** to the data gave the values indicated in Table 1. The smallest value of the coefficient of determination, R^2, was 0.93. In many cases, the junction density increased to a maximum value during the loading period and then gradually decreased to a stable value. For trials d_1 and d_2, however, the junction density continued to increase during the whole contact period. For the finger pressing against the elastomer surface, the evolution of the effective contact area, A_{E}, was so rapid that the kinetics could not be observed. As a result, A_{E} closely tracked the evolution of the normal load, reaching its ultimate value after the load ceased to increase.

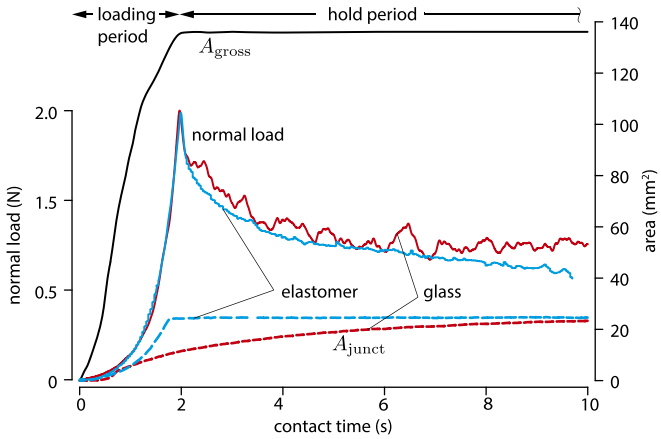

Fig. 2. Typical evolution of the load force, A_{gross}, and A_{junct} as a function of contact time for a glass (red) and for an elastomer (blue) counter surface. The evolution of A_{gross} is independent from the material of the counter surface.

Discussion

Variability. Despite highly controlled testing conditions, there were very large differences in the evolution of the junction contact area between a fingertip and a hard smooth surface, such as glass. During trial b_2, the normalized contact area, A_E, exhibited a large maximum value 10 s after the onset of the hold period before decreasing to a steady value. The junction density increased during the loading period and then decreased to a stable value toward the end of the hold period.

For most trials, the evolution of the junction area followed a first-order kinetics relationship, and the junction density tended to increase during the loading period and to decrease to a steady value near the end of the hold period. For some trials (f_1, d_1, d_2), however, the effective contact area increased in a manner that could not be described by Eq. **1**.

Role of Plasticization. During the loading period, A_{junct} and N naturally increased. The subsequent behavior of these values during the hold period, however, depended on other factors than time, chief among them is the extent to which the stratum corneum became plasticized. Plasticization, which is linked to a decrease of the elastic modulus, is caused by hydration and thus, depends on preexisting moisture before contact and on the rate of secretion of sweat from the pores.

For most trials, the reduction in the junction density during the hold period reflected the slow progress of a coalescence process until complete segments became connected. The changes occurred gradually over the hold period, which suggests that the coalescence process was governed by the rate of transport of sweat from the pores and by subsequent diffusion into the stratum corneum layer. The eventual reduction of the junction contact area for trial b_2 suggests that, in this case, the finger had a high initial level of hydration followed by evaporation of water within the interstitial ridge valleys.

Trial d_1 is an example of a finger that was very dry, both at the onset of contact and subsequently, as can be seen from the very slow rise in the true contact area and in the junction density. At the single-camera pixel level, it is not possible to distinguish between very narrow air gaps and partial contact arising from surface roughness. Hence, for example, in trial d_1, it is possible that microscopic junctions actually existed but were too small to be resolved.

Trials d_2 and f_1 corresponded to fingers that were relatively dry, but the fact that the contact areas increased with the hold time suggests that the stratum corneum was more hydrated than in the case of d_1. Moreover, these trials exhibited a continuous increase in the junction density that must have corresponded to junctions gradually being formed as a result of occlusion but with insufficient moisture softening for junction coalescence to take place.

In complete contrast, variability was almost absent for the trials where a finger pressed onto an elastomeric counter surface, regardless of the state of hydration of the finger. This occurrence is exemplified by trial h. The junction area growth kinetics was so rapid that it could not be resolved by our apparatus.

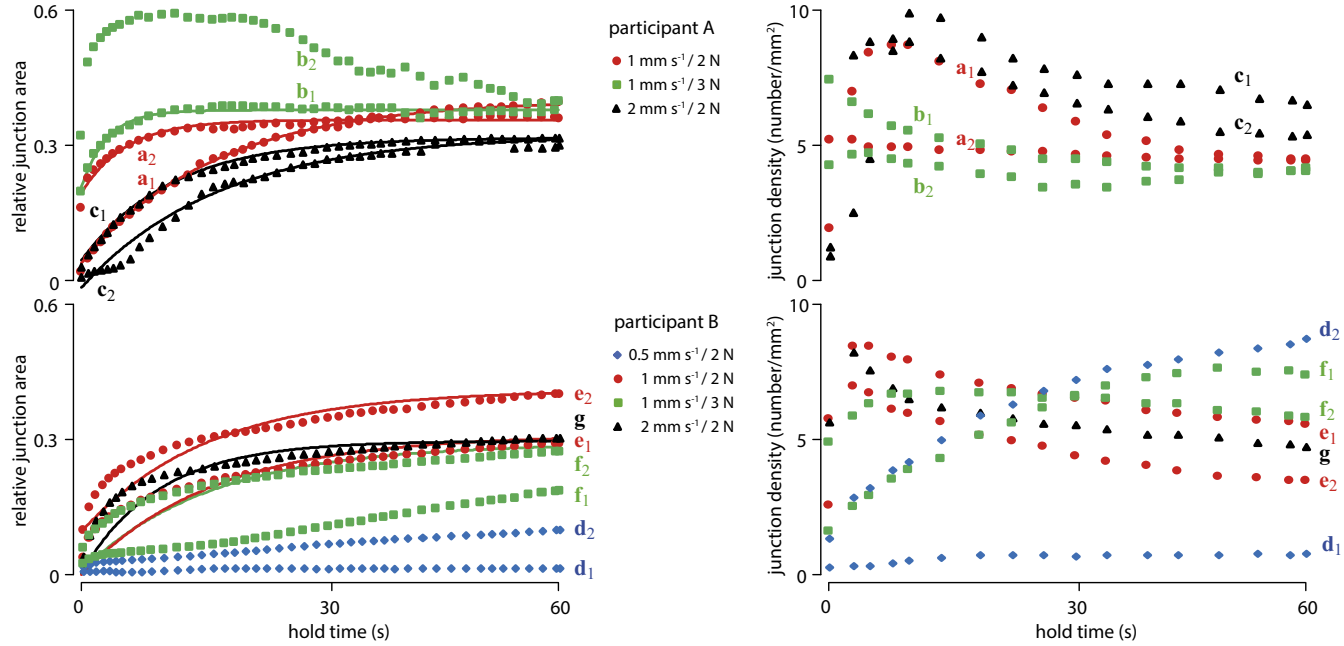

Fig. 3. Evolution of the relative junction area $A_E = A_{junct}/A_{gross}$ and of the junction density N/A_{gross} as a function of hold time in contact with glass for participants A and B and different loading rates and applied loads. Solid lines show first-order kinetics best fits.

Table 1. Experimental protocol loading parameters

	Conditions				Results				
Trials	Rate (mm s^{-1})	Load (N)	Participant	Material	A_0 (mm^2)	A_∞ (mm^2)	λ (s)	t_{max} (s)	A_E ($t = 60$ s)
a_1	1.0	2.0	A	Glass	3.7 ± 0.2	39.5 ± 0.2	16.5 ± 0.3	2.2	0.39
a_2	1.0	2.0	A	Glass	20.9 ± 0.6	38.4 ± 0.2	5.5 ± 0.4	2.8	0.35
b_1	1.0	3.0	A	Glass	19.5 ± 0.5	35.5 ± 0.1	3.2 ± 0.2	2.2	0.37
b_2	1.0	3.0	A	Glass	29.5	—	—	2.4	0.39
c_1	2.0	2.0	A	Glass	4.0 ± 0.9	29.3 ± 1.9	27.0 ± 3.1	1.2	0.30
c_2	2.0	2.0	A	Glass	4.3 ± 0.2	30.9 ± 0.2	11.2 ± 0.3	1.0	0.31
d_1	0.5	2.0	B	Glass	0.7	—	—	3.4	0.01
d_2	0.5	2.0	B	Glass	1.9	—	—	3.3	0.09
e_1	1.0	2.0	B	Glass	7.4 ± 0.4	26.7 ± 0.4	16.2 ± 1.1	1.4	0.27
e_2	1.0	2.0	B	Glass	15.0 ± 0.6	38.6 ± 0.5	15.6 ± 1.3	1.7	0.37
f_1	1.0	3.0	B	Glass	2.6	—	—	1.7	0.17
f_2	1.0	3.0	B	Glass	9.3 ± 0.4	29.1 ± 0.4	16.0 ± 0.1	1.8	0.25
g	2.0	2.0	B	Glass	8.0 ± 0.7	28.2 ± 0.3	9.5 ± 0.8	0.8	0.28
h	1.0	2.0	B	PDMS	25.0 ± 0.1	25.0 ± 0.1	< 0.04	2.4	0.38

Subscripts in trial labels indicate repeated conditions. Results show the values of the best fit parameters to first-order kinetics Eq. **1**. Missing values indicate the absence of a good fit.

Contact Mechanics. As shown in Fig. 1, throughout the evolution of a finger contact against glass, the width of the junctions and of the ridge apices tended to be greater toward the center of the contact area than in the periphery. These differences can be understood by applying Hertz theory at two different length scales: one at the scale of the whole finger and the other at the scale of individual ridges (8). The images of the fingerprint ridges (Fig. 4*A*) thus were generally less dense toward the periphery, which is consistent with a decrease of the Hertzian contact pressure.

The sweat pores caused small regions to remain without contact (white regions in Fig. 1). Thus, even for fully connected ridges, A_{true} was always smaller than A_{ridge}.

Tribology. The adhesion model of friction (23, 24), which has been shown to be applicable to the stratum corneum (25, 26), states that the frictional force, f_f, depends on the product of the interfacial shear strength, τ, and the true area of contact, A_{true}, which is reflected by A_{junct}. The true area of contact measures the amount of intimate, friction-generating contact. Such contacts have transient molecular junctions at the sliding interface.

The frictional force is the work done per unit of sliding distance required to rupture those junctions that transmit stress across the sliding interface and cause subsurface inelastic deformation to a depth of about 100 nm (27). For glassy polymers, the interfacial stress, determined by τ, has been related to surface yielding with values of 1–10 MPa that are about an order of magnitude smaller than those in the bulk, since surface polymer chains have greater freedom to align with the sliding direction (27). Plasticization by water of hydrophilic polymers, such as nylon, is known to cause a reduction in τ in a similar way to that observed for the bulk yield stress (28).

Human fingerprint ridges are decorated with very small-scale surface topographical features that correspond to the asperities of rough surfaces. When compressed, the stratum corneum is initially stiff, and the deformation of the asperities is limited. The increase in the area of existing junctions or ridges and the consequent formation of new asperity contacts with increasing applied normal load, w, are the origin of Coulomb's law, $f_f = \mu w$, where μ is the coefficient of friction.

With time, the asperities become compliant because of the plasticization by moisture, and A_{true} increases. It is reasonable to believe that the stratum corneum behaves like nylon, such that concomitantly, the value of τ decreases as a result of the plasticization. We can model this process by writing $f_f = \tau(t)A_{\text{true}} = \tau(t)\phi(t)A_{\text{junct}}(t \to \infty)$, where $A_{\text{junct}}(t \to \infty)$ is the steady-state contact area of the junctions, including those that have coalesced to form whole-ridge segments. The scalar quantity, $\phi(t)$, varies between zero just before contact and unity at long times after asperity junctions no longer grow in size and number.

Sliding on Impermeable, Hard Surfaces. We observed previously that the value of the coefficient of friction, μ, for a finger pad sliding on a smooth glass surface also increased with the contact time, because the increase in A_{true} is greater than the decrease in τ (20). The value of μ can increase by up to an order of magnitude for small normal loads, and its evolution at a constant normal load can be described by a first-order kinetics relationship with a characteristic time of up to 20 s (29). Thus, it is probable that $\phi(t)$ generally exhibits a similar behavior, but a technique able to reliably measure A_{true} for rough surfaces has yet to developed.

We also previously reported that, with increasing contact time, the friction of a finger pad gradually changes from Coulombic to a nonlinear dependence on a normal load in a manner that is typical of elastomers, when the asperities are sufficiently compliant to flatten under the applied load (29). This phenomenon is a direct result of a glassy–rubbery transition of the stratum corneum caused by the moisture-driven plasticization. Thus, in the fully occluded state, $A_{\text{true}} \approx A_{\text{junct}}$.

Sliding on Soft Surfaces. The surprisingly slow formation of a true contact between a finger pad and a hard, smooth, and impermeable surface, such as glass, may be contrasted with the case of a counter surface made of a compliant material, such as a rubber or an elastomer (e.g., PDMS), as further illustrated by the "true contact" images in Fig. 4*A* that were acquired with the same finger measured under similar conditions but with a different material. Fig. 4*C* illustrates the stability of finger contacts with an elastomeric surface through time.

Fig. 4*B* shows the evolution of μ when a finger pad slid on a smooth elastomeric surface (PDMS: Young's elastic modulus $E = 2.3$ MPa; estimated Young's elastic modulus of keratin: $E \approx 1$ GPa in a dry state) and on a glass surface. For PDMS, the coefficient of friction was nearly constant throughout the contact time, while a first-order kinetic relationship of the form of Eq. **1** could be successfully fitted in the case of a glass surface.

Confounds Caused by Water Are Unlikely. The grayscale images in Fig. 4*A* show a few dark spots that may be ascribed to the

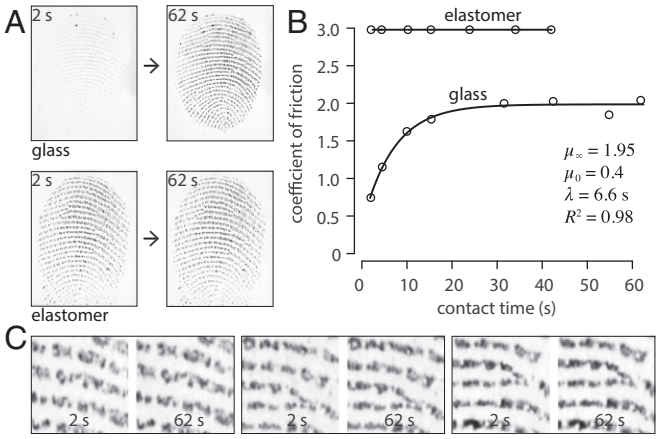

Fig. 4. (*A*) Contrasted kinetics of contact formation for a peak compression of 2 N showing images at the beginning and end of the subsequent hold period. (*B*) Time course of the evolution of friction for a finger sliding on an elastomeric surface or on a glass surface (fitted to a first-order kinetic relationship) at a velocity of 0.02 m s^{-1} and under a load of 0.2 N. (*C*) Pairs of enlarged grayscale images from randomly selected trials with an elastomeric surface.

presence of water droplets, raising the concern that the true contact area could be confounded by the occurrence of water bridges in interstitial spaces and cause an overestimation of the true contact area. The presence of water, however, could not explain the increase of the coefficient by a factor of five over a period of 20 s as shown by Fig. 4*B*. Free moisture would be expected to lead to a reduction of the friction. Moreover, taking steps to eliminate the presence of liquid water, the dark regions between (forearm) skin and a transparent window observed in high-resolution Raman microscopy have also indicated the presence of solid–solid junctions (30).

Implications for the Motor and the Perceptual Functions of Touch. The dramatic differences in true contact formation kinetics according to the material properties and to the microtopology of the counter surface have obvious implications for motor behavior. We intuitively feel that elastic rubbery surfaces, even if they are only thin coatings, provide us with a better grip than hard and smooth surfaces. Conversely, the kinematic and tonic motor behavior required to explore surfaces is crucially dependent on the nature of these surfaces. Push too hard on a surface made of a compliant material, and the finger will become stuck. Conversely, clean glass surfaces will remain slippery within the first 10 s of contact regardless of their topology, especially in dry ambient conditions. Each of these cases requires fine and flexible motor control strategies for the successful completion of motor or perceptual tasks.

The kinetics of true contact formation are also likely to be impacted by the hydrophobicity of the material of the counter surface. In fact, some of us have recently shown that people can discriminate materials by touch on the sole basis of hydrophobicity differences (6). Thus, we can tentatively suggest that the contact formation kinetics divide the tactile world into broad categories of materials: smooth and impermeable surfaces that could be subdivided into those that are hard (glass, glazings, polished metals) or those that are softer than keratin (rubbers, certain polymers); rough surfaces that can also be divided into those that are made of relatively hard and soft materials; and porous surfaces (paper, wood, fabrics) that further modify the kinetics of contact formation together with hydrophobicity. For example, it has been observed that, for filter paper, the friction and hence, A_{true} decrease with the contact time, since the secreted sweat is absorbed, leading to reduction in the compliance of the keratin (2).

It can, therefore, be argued that each of these factors potentially conveys reliable tactile information to the brain pertaining to the nature of the touched objects during tactile exploration.

Implications for Tactile Displays Relying on Friction. The modulation of friction by the application of ultrasonic vibration or by electrostatic adhesion is a leading technological option for flat-screen haptic displays (31, 32). They rely on the ability to reduce or augment the overall friction of the screen. The illusion of a ridge (33) may be created by rapidly increasing friction during the exploration by a finger as a result of decreasing the amplitude of vibration or increasing the electrostatic field (3). The strength and stability of this effect are dependent on the contrast in friction that can be induced, which has critical implications for power requirements (34, 35).

The drastic variations of the evolution of A_{junct} with contact time as was observed here for just two participants in a single day are indicative of the variations that might typically be expected for the corresponding intrinsic friction of touch screens. This variation extends to the increase in μ with time, while the data for the glass in Fig. 4*B* correspond to an increase of about a factor of five. Our findings are indeed consistent with the variations in values of the coefficient of friction that are reported in the literature (2, 36, 37). Thus, if the intrinsic friction between a finger pad and screen is small, greater vibrational amplitudes or greater electrostatic voltage swings will be required. Clearly, our findings present a significant challenge to the design of haptic interfaces based on friction modulation in terms of maintaining acceptable fidelity without excessive power requirements.

Materials and Methods

Data Acquisition. The frustrated total internal reflection technique (10, 19) was used to measure the contact area between a finger pad and a glass prism; a schematic diagram of the apparatus is shown in Fig. S1 together with a grayscale rendering of a fingerprint image obtained from the apparatus. Light rays from a diffuse light source were entirely reflected by the internal face of the prism unless there was intimate contact with an object, resulting in a dark image against a light background. The left index fingers of two female volunteers (27 and 26 y old), denoted as participants A and B, were inclined at an angle of 30° with the finger pad facing upward. The glass prism was pressed down via a 10-N load transducer onto the finger pad using a material testing machine to induce frustrated total internal reflection. For the elastomer contact studies, a smooth transparent block of PDMS (Sylgard 184) was adhered to the imaging face of the prism. Initially, the fingers were washed with commercial soap, rinsed with distilled water, and allowed to dry for 10 min until an equilibrated clean skin state was achieved. The contact was imaged through the internal face of the prism using a Nikon D5300 camera with a video resolution of 1,920 × 1,080 pixels at 25 frames per second and a shutter speed of 1/160 s. All measurements were carried out in a single day and in an environmentally controlled laboratory set to 20°C and 50% relative humidity. Additional detail is available in *SI Materials and Methods*. The protocols adopted for finger pad compression and for imaging were approved by the Unilever Research and Development Port Sunlight Independent Ethics Committee, and the volunteers gave informed consent.

Image Processing. Using the ImageJ software (38), image analysis was carried out to determine A_{junct} as a function of the contact duration. Grayscale (eight-bit) conversion and analysis were applied. The converted images were adjusted to the level of contrast and brightness that allowed for optimal pattern recognition. Typical methods were adopted for automatic fingerprint feature extraction (39) and followed a sequence of steps comprising image enhancement, binarization, thinning, extraction, and postprocessing. It was possible to exclude the sweat pores and to determine the size and evolution of each feature by segmenting the image into features of interest from the background under each relevant condition by use of a mask function. To estimate the junction area, a threshold of the grayscale value was determined from the histogram (>75% saturation of the pixel intensities) that allowed the boundaries of the contact junctions to be delineated. The boundary of each junction excluded sweat pores at the edge of the contact

region, but it was not possible to exclude automatically those that were internal to the boundaries. It was estimated that the overestimation of the contact area was $<5\%$, since such internal sweat pores represented a relatively small proportion of the total contact area, particularly because they were only present in the central region of the fingerprint images.

ACKNOWLEDGMENTS. The study was funded by FP7 Marie Curie Initial Training Network Virtual Prototyping of Tactile Displays Grant 317100. It was also supported by European Research Council (FP7) European Research Council Advanced Grant (Computational Theory of Haptic Perception) 247300 (to V.H.).

1. Dyson J, Hirst W (1954) The true contact area between solids. *Proc Phys Soc B* 67: 309–312.
2. Pasumarty SM, Johnson SA, Watson SA, Adams MJ (2011) Friction of the human finger pad: Influence of moisture, occlusion and velocity. *Tribol Lett* 44:117–137.
3. Vezzoli E, et al. (2015) Physical and perceptual independence of ultrasonic vibration and electrovibration for friction modulation. *IEEE Trans Haptics* 8:235–239.
4. Wiertlewski M, Friesen RF, Colgate JE (2016) Partial squeeze film levitation modulates fingertip friction. *Proc Natl Acad Sci USA* 113:9210–9215.
5. Nakatani M, Howe RD, Tachi S (2011) Surface texture can bias tactile form perception. *Exp Brain Res* 208:151–156.
6. Gueorguiev D, Bochereau S, Mouraux A, Hayward V, Thonnard JL (2016) Touch uses frictional cues to discriminate flat materials. *Sci Rep* 6:25553.
7. McKittrick J, et al. (2012) The structure, functions, and mechanical properties of keratin. *JOM* 64:449–445.
8. Dzidek BM, Adams MJ, Andrews JW, Zhang Z, Johnson SA (2017) Contact mechanics of the human finger pad under compressive loads. *J R Soc Interf* 14:20160935.
9. Wildnauer RH, Bothwell JW, Douglass AB (1971) Stratum corneum biomechanical properties, I. Influence of relative humidity on normal and extracted human stratum corneum. *J Investig Dermatol* 56:72–78.
10. Lévesque V, Hayward V (2003) Experimental evidence of lateral skin strain during tactile exploration. *Proceedings of EuroHaptics*, eds Oakley I, O'Modhrain S, Newell F (Eurohaptics Society, Paris), pp 261–275.
11. Tada M, Mochimaru M, Kanade T (2006) How does a fingertip slip?—visualizing partial slippage for modeling of contact mechanics. *Proceedings of EuroHaptics*, eds Andriot C, Gentaz E, Iwata H, Salcudean T (Eurohaptics Society, Paris), pp 415–420.
12. Warman PH, Ennos AR (2009) Fingerprints are unlikely to increase the friction of primate fingerpads. *J Exp Biol* 212:2015–2021.
13. Adams MJ, et al. (2013) Finger pad friction and its role in grip and touch. *J R Soc Interf* 10:20120467.
14. André T, Lefèvre P, Thonnard JL (2009) A continuous measure of fingertip friction during precision grip. *J Neurosci Meth* 179:224–229.
15. André T, Levèsque V, Hayward V, Lefèvre P, Thonnard JL (2011) Effect of skin hydration on the dynamics of fingertip gripping contact. *J R Soc Interf* 8:1574–1583.
16. Delhaye B, Lefèvre P, Thonnard JL (2014) Dynamics of fingertip contact during the onset of tangential slip. *J R Soc Interf* 11:20140698.
17. Terekhov AV, Hayward V (2011) Minimal adhesion surface area in tangentially loaded digital contacts. *J Biomech* 44:2508–2510.
18. Soneda T, Nakano K (2010) Investigation of vibrotactile sensation of human finger pads by observation of contact zones. *Tribol Int* 43:210–217.
19. Bochereau S, Dzidek B, Adams MJ, Hayward V (July 4, 2017) Characterizing and imaging gross and real finger contacts under dynamic loading. *IEEE Trans Haptics*, 10.1109/TOH.2017.2686849.
20. Dzidek BM, Bochereau S, Johnson S, Hayward V, Adams MJ (2016) Frictional dynamics of finger pads are governed by four length-scales and two time-scales. *Proceedings of the Haptics Symposium*, eds Choi S, Kuchenbecker KJ, Gerling G (IEEE, Piscataway, NJ), pp 161–166.
21. O'Leary E, Slaney J, Bryant DG, Fraser FC (1986) A simple technique for recording and counting sweat pores on the dermal ridges. *Clin Genet* 29:122–128.
22. Pawluk DTV, Howe RD (1999) Dynamic contact of the human fingerpad against a flat surface. *J Biomech Eng* 121:605–611.
23. Amuzu JKA, Briscoe BJ, Tabor D (1977) Friction and shear strength of polymers. *ASLE Trans* 20:354–358.
24. Briscoe BJ, Arvanitaki A, Adams MJ, Johnson SA (2001) The friction and adhesion of elastomers. *Tribol Ser* 39:661–672.
25. Johnson SA, Gorman DM, Adams MJ, Briscoe BJ (1993) The friction and lubrication of human stratum corneum. *Tribol Ser* 25:663–672.
26. Adams MJ, Briscoe BJ, Johnson SA (2007) Friction and lubrication of the human skin. *Tribol Lett* 26:239–253.
27. Briscoe BJ, Smith AC (1981) Polymer friction and polymer yield: A comparison. *Polymer* 22:1587–1589.
28. Cohen SC, Tabor D (1966) The friction and lubrication of polymers. *Proc Roy Soc Lond A* 291:186–207.
29. Dzidek BM, et al. (2014) Role of occlusion in non-coulombic slip of the finger pad. *EuroHaptics: Neuroscience, Devices, Modeling, and Applications*, eds Auvray M, Duriez C (Springer, Berlin), pp 109–116.
30. Dąbrowska AK, et al. (2016) In vivo confirmation of hydration-induced changes in human-skin thickness, roughness and interaction with the environment. *Biointerphases* 11:031015.
31. Giraud F, Amberg M, Lemaire-Semail B, Casiez G (2012) Design of a transparent tactile stimulator. *Proceedings of the Symposium on Haptic Interfaces for Virtual Environment and Teleoperator Systems*, MacLean K., O'Maley MK (IEEE, Piscataway, NJ), pp 485–489.
32. Meyer D, Peshkin M, Colgate JE (2013) Fingertip friction modulation due to electrostatic attraction. *Proceedings of the World Haptics Conference*, eds Tan HZ, Otaduy MA, Shinoda H (IEEE, Piscataway, NJ), pp 43–48.
33. Robles De La Torre G, Hayward V (2001) Force can overcome object geometry in the perception of shape through active touch. *Nature* 412:445–448.
34. Vezzoli E, et al. (2017) Friction reduction through ultrasonic vibration part 1: Modelling intermittent contact. *IEEE Trans Haptics* 10:208–216.
35. Sednaoui T, et al. (2017) Friction reduction through ultrasonic vibration part 2: Experimental evaluation of intermittent contact and squeeze film levitation. *IEEE Trans Haptics* 10:208–216.
36. Derler S, Rotaru GM (2013) Stick-slip phenomena in the friction of human skin. *Wear* 301:324–329.
37. Urbakh M, Klafter J, Gourdon D, Israelachvili J (2004) The nonlinear nature of friction. *Nature* 430:525–528.
38. ImageJ (2016) ImageJ2, Version 1.4Oi. Available at https://imagej.net/Welcome. Accessed September 2017.
39. Domeniconi C, Tari S, Liang P (1998) Direct gray scale ridge reconstruction in fingerprint images. *Proceedings of the IEEE International Conference on Acoustics Speech and Signal Processing* (IEEE, Piscataway, NJ), pp V–2941.